

## Nitric Acid Uptake on Subtropical Cirrus Cloud Particles

2

4

P.J. Popp\*, R.S. Gao, T.P. Marcy\*, D.W. Fahey\*, P.K. Hudson\*, T.L. Thompson  
*Aeronomy Laboratory, National Oceanic and Atmospheric Administration  
Boulder, CO 80305*

8

*\*Cooperative Institute for Research in Environmental Sciences, University of Colorado*

10

B. Kärcher  
*Institut für Physik der Atmosphäre, Deutsches Zentrum für Luft- und Raumfahrt  
Oberpfaffenhofen, Germany*

12

14

B.A. Ridley, A.J. Weinheimer, D.J. Knapp, D.D. Montzka  
*Atmospheric Chemistry Division, National Center for Atmospheric Research  
Boulder, CO 80307*

16

18

D. Baumgardner  
*Universidad Nacional Autonoma de Mexico, Centro de Ciencias de la Atmosfera  
Ciudad Universitaria, 04510 Mexico DF, Mexico*

20

22

T.J. Garrett  
*Department of Meteorology, University of Utah  
Salt Lake City, UT 84112*

24

26

E.M. Weinstock, J.B. Smith, D.S. Sayres, J.V. Pittman  
*Atmospheric Research Project, Harvard University  
Cambridge, MA 02138*

28

30

S. Dhaniyala  
*Division of Geology and Planetary Sciences, California Institute of Technology  
Pasadena, CA 91125  
Now at Department of Mechanical and Aeronautical Engineering, Clarkson University  
Potsdam, NY 13699*

32

34

36

T.P. Bui  
*NASA Ames Research Center  
Moffett Field, CA 94035*

38

40

M.J. Mahoney  
*Jet Propulsion Laboratory, California Institute of Technology  
Pasadena, CA 91109*

42

## Abstract

2        The redistribution of HNO<sub>3</sub> via uptake and sedimentation by cirrus cloud particles is  
considered an important term in the upper tropospheric budget of reactive nitrogen.  
4        Numerous cirrus cloud encounters by the NASA WB-57F high-altitude research aircraft  
during CRYSTAL-FACE were accompanied by the observation of condensed-phase  
6        HNO<sub>3</sub> with the NOAA chemical ionization mass spectrometer. The instrument measures  
HNO<sub>3</sub> with two independent channels of detection connected to separate forward- and  
8        downward-facing inlets that allow a determination of the amount of HNO<sub>3</sub> condensed on  
ice particles. Subtropical cirrus clouds, as indicated by the presence of ice particles, were  
10        observed coincident with condensed-phase HNO<sub>3</sub> at temperatures of 197 K - 224 K and  
pressures of 122 hPa - 224 hPa. Maximum levels of condensed-phase HNO<sub>3</sub> approached  
12        the gas-phase equivalent of 0.8 ppbv. Ice particle surface coverages as high as  $1.4 \cdot 10^{14}$   
molecules·cm<sup>-2</sup> were observed. A dissociative Langmuir adsorption model, when using  
14        an empirically derived HNO<sub>3</sub> adsorption enthalpy of -11.0 kcal·mol<sup>-1</sup>, effectively  
describes the observed molecular coverages to within a factor of 5. The percentage of  
16        total HNO<sub>3</sub> in the condensed phase ranged from near zero to 100% in the observed cirrus  
clouds. With volume-weighted mean particle diameters up to 700 μm and particle fall  
18        velocities up to 10 m·s<sup>-1</sup>, some observed clouds have significant potential to redistribute  
HNO<sub>3</sub> in the upper troposphere.

## 1. Introduction

2       Cirrus clouds are ubiquitous throughout the upper troposphere (UT) and can cover as  
much as 40% of the Earth's surface [Liao *et al.*, 1995, Jin *et al.*, 1996, Wang *et al.*, 1996,  
4       Wylie and Menzel, 1999]. Composed of ice crystals [Lynch, 2002], cirrus clouds are  
known to play a complex and significant role in the global radiation budget [Liou, 1986].  
6       Cirrus clouds can be formed in situ in the UT [Kärcher, 2002], as a result of synoptic  
weather disturbances, or in the anvil outflow at the top of cumulonimbus clouds [Sassen,  
8       2002]. Tropical cirrus clouds around the peak convective detrainment level are formed  
primarily via the latter mechanism, and can reach altitudes of up to 18 km when produced  
10      in deep convective systems. The broad lateral and vertical extent of anvil cirrus clouds  
produced in the tropics is expected to exert a greater influence on the Earth's climate  
12      system than midlatitude cirrus [Heymsfield and McFarquhar, 2002]. Due to the high  
altitudes and often-remote locations of tropical cirrus, however, comprehensive in situ  
14      measurements of these clouds have been limited.

Model simulations by Lawrence and Crutzen [1998] suggest that the uptake and  
16      gravitational redistribution of nitric acid ( $\text{HNO}_3$ ) by cirrus cloud particles may represent  
a significant sink of  $\text{HNO}_3$  in the UT. Nitric acid serves as a primary reservoir species  
18      for nitrogen oxides ( $\text{NO}_x$ ) [Neuman *et al.*, 2001], which are directly involved in the  
photochemical production of tropospheric ozone [Jaeglé *et al.*, 1998]. Model studies of  
20      cirrus-processed air have demonstrated that the sedimentary removal of  $\text{HNO}_3$  from the  
UT can effect strong local reductions in  $\text{NO}_x$ , with the consequence of significant  
22      reductions in the net ozone production rate [Meier and Hendricks, 2002]. Since ozone is  
known to be an effective greenhouse gas in the troposphere [Albritton *et al.*, 2001],  
24      particularly near the tropopause [Lacis *et al.*, 1990], understanding the uptake and  
redistribution of  $\text{HNO}_3$  by cirrus cloud particles may be important in assessing the  
26      contribution of cirrus clouds to the radiative forcing of climate change.

A number of laboratory studies have investigated the uptake of  $\text{HNO}_3$  on ice surfaces

at temperatures typical of the UT. Experiments performed by *Zondlo et al.* [1997] on  
2 vapor-deposited ice films at 211 K resulted in observed HNO<sub>3</sub> surface coverages of  
1.5·10<sup>15</sup> molecules·cm<sup>-2</sup>. A series of similar experiments reported by *Hudson et al.*  
4 [2002] at an HNO<sub>3</sub> pressure ( $P(\text{HNO}_3)$ ) of 1.1·10<sup>-6</sup> hPa indicated a negative temperature  
dependence to the observed uptake, with coverages of 1.1·10<sup>14</sup> to 5.9·10<sup>13</sup> molecules·cm<sup>-</sup>  
6 <sup>2</sup> over a temperature range of 214-220 K. Uptake studies performed on ice films by  
*Abbatt* [1997] yielded coverages of up to 2.9·10<sup>14</sup> molecules·cm<sup>-2</sup> at temperatures as low  
8 as 208 K, with no apparent dependency on  $P(\text{HNO}_3)$  values over the range 1.7·10<sup>-7</sup> to  
4.1·10<sup>-6</sup> hPa. *Hynes et al.* [2002] reported comparable coverages using a similar  
10 technique, although they observed coverages increasing by factor of 2 over a nearly 10-  
fold increase in  $P(\text{HNO}_3)$ , from 5.0·10<sup>-7</sup> - 3.0·10<sup>-6</sup> hPa. A laboratory study of HNO<sub>3</sub>  
12 uptake on nebulized half-micron diameter ice particles at 230 K yielded coverages similar  
to those observed on the ice films (1.2·10<sup>14</sup> molecules·cm<sup>-2</sup>), although these experiments  
14 were performed at the relatively high  $P(\text{HNO}_3)$  of 7·10<sup>-6</sup> hPa [*Arora et al.*, 1999]. There  
has not yet been an extensive laboratory study of HNO<sub>3</sub> uptake on ice surfaces performed  
16 at  $P(\text{HNO}_3)$  values typical of the UT (< 2.0·10<sup>-7</sup> hPa).

Prior field studies of HNO<sub>3</sub> uptake on cirrus cloud particles have been made at mid  
18 and high latitudes. Measurements of total reactive nitrogen (NO<sub>y</sub> = NO + NO<sub>2</sub> + 2N<sub>2</sub>O<sub>5</sub>  
+ HNO<sub>3</sub> + ...) in a mountain wave cloud over the continental United States reported by  
20 *Weinheimer et al.* [1998] indicated that levels of condensed NO<sub>y</sub> in the cloud approached  
20% of total NO<sub>y</sub>. Surface coverages on the wave cloud ice particles were calculated to  
22 be as high as 2.5·10<sup>13</sup> molecules·cm<sup>-2</sup> [*Hudson et al.*, 2002]. Measurements of  
condensed-phase NO<sub>y</sub> in cirrus layers in the Arctic UT by *Kondo et al.* [2003] yielded  
24 HNO<sub>3</sub> coverages as high as 1.6·10<sup>14</sup> molecules·cm<sup>-2</sup> at temperatures of approximately  
200 K, with coverages decreasing at warmer temperatures. *Meilinger et al.* [1999]  
26 conducted similar measurements in Arctic cirrus clouds at 196 K and reported coverages  
of only 1·10<sup>13</sup> molecules·cm<sup>-2</sup>. An extensive dataset of measurements made at

midlatitudes revealed median levels of condensed  $\text{NO}_y$  (assumed to be  $\text{HNO}_3$ ) in the northern hemisphere of  $3.6 \cdot 10^{12}$  molecules $\cdot\text{cm}^{-2}$  to be greater than twice that observed in the southern hemisphere [Ziereis *et al.*, 2003]

We report here an extensive dataset of in situ measurements, including gas- and condensed-phase  $\text{HNO}_3$  and ice particle surface area density (SAD), obtained in subtropical in situ and anvil cirrus clouds. These measurements were conducted onboard the NASA WB-57F high-altitude research aircraft as part of the Cirrus Regional Study of Tropical Anvils and Cirrus Layers Florida Area Cirrus Experiment (CRYSTAL-FACE) mission. The data are used here to assess the uptake of  $\text{HNO}_3$  by subtropical cirrus cloud particles and explore the partitioning of  $\text{HNO}_3$  between the gas and ice particle phases in cirrus clouds.

## 2. Instrumentation

This study utilizes data from a number of in situ instruments onboard the NASA WB-57F aircraft. Gas-phase and condensed-phase  $\text{HNO}_3$  measurements made by chemical ionization mass spectrometry are described in more detail below. Particle size distribution and number density measurements made by the Cloud, Aerosol and Precipitation Spectrometer (CAPS) were used to derive SAD and volume-weighted mean diameter (VMD) for ice particles in the size range between 0.35-1550  $\mu\text{m}$  [Baumgardner *et al.*, 2001]. Note that all particle sizes cited herein refer to particle diameter, and not radius. A second, independent measurement of SAD was provided by the Cloud Integrating Nephelometer (CIN) [Gerber *et al.*, 2000]. Ice water content (IWC) and water ( $\text{H}_2\text{O}$ ) vapor were measured by the Harvard University Lyman- $\alpha$  hygrometer [Weinstock *et al.*, 1994, Weinstock *et al.*, 2003]. Nitric oxide (NO) and total reactive nitrogen ( $\text{NO}_y$ ) were measured by catalytic reduction and chemiluminescence [Weinheimer *et al.*, 2003]. Ambient temperature and pressure, and WB-57F true air speed were measured by the Meteorological Measurement System (MMS) [Scott *et al.*, 1990]. The precision and accuracy of these measurements are summarized in Table 1.

Tropopause height was measured by the microwave temperature profiler (MTP)  
[Denning *et al.*, 1989].

## 2.1. HNO<sub>3</sub> Measurements

HNO<sub>3</sub> was measured using the NOAA chemical ionization mass spectrometer (CIMS) located in the third pallet position of the NASA WB-57F aircraft. This instrument measures HNO<sub>3</sub> with an accuracy of  $\pm 20\%$  and precision of 30 pptv ( $1\sigma$ , 10-s averages), and has been described in detail elsewhere [Neuman *et al.*, 2000]. Prior to CRYSTAL-FACE, the NOAA CIMS was modified by the addition of a second independent channel for the measurement of HNO<sub>3</sub> and the relocation of the original sample inlet on the CIMS inlet pylon (Fig. 1). The two CIMS channels are designed to provide identical measurements of gas-phase HNO<sub>3</sub>. Due to differences in the particle sampling efficiencies of the two inlets, however, the two channels have different sensitivity to condensed-phase HNO<sub>3</sub>. When sampling in cirrus clouds, the forward-facing front inlet samples both gas-phase HNO<sub>3</sub> and any HNO<sub>3</sub> condensed on the cirrus particles. The downward-facing bottom inlet samples primarily gas-phase HNO<sub>3</sub> because the plane of the sampling orifice is parallel to the direction of flow over the inlet, which is set by the flow straightener. Semi-empirical calculations indicate that approximately 50% of 0.1  $\mu\text{m}$  particles and greater than 90% of 1  $\mu\text{m}$  and larger particles are inertially stripped from the air sampled by the bottom inlet [Vincent *et al.*, 1986]. Calculations further suggest that ice particles greater than 10  $\mu\text{m}$  in diameter (typical of cirrus clouds observed during CRYSTAL-FACE) are almost entirely removed from the sampled air. Thus, for most of the cirrus clouds sampled, the HNO<sub>3</sub> from the bottom inlet is taken to be a measure of the gas-phase HNO<sub>3</sub> abundance.

The conclusion that ice particles greater than approximately 1  $\mu\text{m}$  are inertially separated from air sampled by the bottom inlet is further supported by measurements made in the contrail of the WB-57F during CRYSTAL-FACE. The contrail contained ice particles with high number densities (100-200  $\text{cm}^{-3}$ ) and volume-weighted mean

diameters on the order of  $2 \mu\text{m}$  [Gao *et al.*, 2003].  $\text{HNO}_3$  was present in the contrail  
2 because of mixing between the exhaust gases and ambient air containing approximately  
0.4 ppbv  $\text{HNO}_3$ . Measurements in the contrail as soon as 4 minutes after formation  
4 indicated a difference between the front and bottom CIMS channels. The minimum  
signal from the bottom channel was near zero inside the contrail. This low  $\text{HNO}_3$  signal  
6 is consistent with the removal of gas-phase  $\text{HNO}_3$  by uptake onto the  $2\text{-}\mu\text{m}$  ice particles  
in the contrail, and the inertial stripping of these particles from the bottom inlet sample  
8 flow. As expected, a simultaneous increase in  $\text{HNO}_3$  above ambient values occurred in  
the front CIMS channel, which does not discriminate against  $2 \mu\text{m}$  particles. If the  
10 bottom CIMS inlet sampled  $2 \mu\text{m}$  particles with any significant efficiency,  $\text{HNO}_3$   
observed in the bottom channel during the contrail intercept would not be significantly  
12 lower than the ambient values immediately outside the contrail.

The front CIMS inlet samples subisokinetically, meaning the sample air velocity  
14 inside the inlet ( $U$ ) is less than the WB-57F true air speed ( $U_0$ ) of  $140\text{-}200 \text{ m}\cdot\text{s}^{-1}$  at  
sampling altitudes. As a result, cirrus cloud particle number densities in the sampled air  
16 stream are inertially enhanced relative to those in the ambient air. A computational fluid  
dynamics program (Fluent Inc., New Hampshire) was used to estimate particle  
18 enhancement factors ( $EF$ ) in the front inlet by simulating the flow field and particle  
trajectories around a two-dimensional horizontal cross section of the CIMS pylon and  
20 inlet structure (Fig. 1). The value of  $EF$  is near unity for small particles ( $< 0.1 \mu\text{m}$ ) and  
increases with particle size, as found for similar configurations [Northway *et al.*, 2002].  
22 For particles larger than approximately  $10 \mu\text{m}$  in diameter, typical of cirrus cloud ice  
particles sampled during CRYSTAL-FACE,  $EF$  for the front inlet approaches the  
24 maximum value of  $U_0/U$ . Since both CIMS channels sample at a constant mass flow of  
 $1.85$  standard liters per minute (slpm),  $U$ , and therefore,  $EF$ , are dependent upon the  
26 ambient temperature and pressure. Under typical WB-57F sampling conditions during  
CRYSTAL-FACE (temperature =  $213 \text{ K}$ , pressure =  $170 \text{ hPa}$ ,  $U_0 = 200 \text{ m}\cdot\text{s}^{-1}$ ),  $EF$  has a

maximum value of approximately 16.

2        Cirrus cloud particles entering the front CIMS inlet travel through a 20 cm length of  
Teflon™ tubing (6.4 mm outside diameter, 4.0 mm inside diameter) upstream of the  
4        CIMS flow control valve and flow tube (Fig. 1). The use of Teflon™ sample lines  
ensures that HNO<sub>3</sub> will not readily absorb on the inlet surfaces [Neuman *et al.*, 1999].  
6        This tubing, which is heated to 48° C in flight, has two bends to help ensure that large  
particles entering the inlet will impact on the tubing walls and subsequently evaporate  
8        prior to reaching the flow control valve. Particles with diameters greater than  
approximately 20 μm have large enough stopping distances at the freestream velocity that  
10       they impact at the first bend. Some particles that do not fully evaporate will impact in the  
body of the flow control valve or the flow tube entrance. HNO<sub>3</sub> condensed on the  
12       particle surfaces is liberated to the gas phase early in the evaporation process and  
measured as a gas-phase equivalent volume mixing ratio. The HNO<sub>3</sub> mixing ratio  
14       measured by the front CIMS channel, therefore, represents the sum of the gas- and the  
condensed-phase values, with the condensed-phase component enhanced by the value of  
16       *EF*.

### 3. Observations

18       Condensed-phase HNO<sub>3</sub> was observed coincident with cirrus cloud observations on 4  
WB-57F science flights conducted as part of CRYSTAL-FACE. These flights  
20       originated and terminated at the United States Naval Air Facility, Key West (24.6° N,  
81.7° W) in Florida on July 11, 13, 19 and 21, 2002. Time series data of HNO<sub>3</sub> mixing  
22       ratios observed from the front and bottom CIMS channels (HNO<sub>3|front</sub> and HNO<sub>3|gas</sub>,  
respectively), as well as particle SAD, IWC (represented as a gas-phase equivalent  
24       volume mixing ratio) and meteorological parameters are shown for July 11, 13, 19 and 21  
in Figs. 2-5, respectively. The presence of cirrus cloud particles is indicated by increases  
26       in SAD and IWC above background values. The presence of condensed-phase HNO<sub>3</sub> in  
a flight segment is indicated by HNO<sub>3|front</sub> values that are significantly greater than

HNO<sub>3</sub>|<sub>gas</sub> values. Flight segments identified by purple bars in panel (b) for July 13 (Fig. 3) and July 19 (Fig. 4) represent the observation of contrail cirrus clouds. As stated previously, these clouds are characterized by having high particle number densities with volume-weighted mean diameters typically much lower than cirrus clouds formed by natural processes. Due to the uncertainties in the SAD measurements in the contrail-formed cirrus clouds and in the value of  $EF$  for particles in this size range, these clouds are not considered in the data analysis presented here.

Cirrus clouds were observed from the WB-57F at pressures between 122 hPa and 224 hPa during the flights of July 11, 13, 19 and 21, corresponding to pressure altitudes between 11 km and 15 km (Figs. 2-5). These clouds were observed at temperatures between 197 K and 224 K. Figures 2-5 show the strong temporal correlation of (HNO<sub>3</sub>|<sub>front</sub> - HNO<sub>3</sub>|<sub>gas</sub>) with both SAD and IWC in cirrus clouds, with HNO<sub>3</sub>|<sub>gas</sub> approaching zero during a number of cirrus events. Outside of clouds, measured values of HNO<sub>3</sub>|<sub>front</sub> and HNO<sub>3</sub>|<sub>gas</sub> generally agree well (with an overall correlation coefficient,  $r$ , of 0.92). However, some periods in Figs. 2-5 show offsets between the two channels that are best explained as changes in the inlet line surfaces during the flight. Figure 4 also indicates elevated values of relative humidity (with respect to ice) during a number of cirrus cloud encounters, as described by *Gao et al.* [2003].

Condensed-phase HNO<sub>3</sub>, proportional to the difference between the values of HNO<sub>3</sub>|<sub>front</sub> and HNO<sub>3</sub>|<sub>gas</sub>, was observed primarily at SADs greater than 200  $\mu\text{m}^2\cdot\text{cm}^{-3}$  during CRYSTAL-FACE (Fig. 6). Note that for the values of (HNO<sub>3</sub>|<sub>front</sub> - HNO<sub>3</sub>|<sub>gas</sub>) shown in Fig. 6, HNO<sub>3</sub>|<sub>front</sub> is not corrected for particle oversampling. Values of (HNO<sub>3</sub>|<sub>front</sub> - HNO<sub>3</sub>|<sub>gas</sub>) at SADs less than 200  $\mu\text{m}^2\cdot\text{cm}^{-3}$  are near the detection limit and highly variable due to CIMS instrument noise. In the analyses presented here, observations at SADs greater than 200  $\mu\text{m}^2\cdot\text{cm}^{-3}$  are selected to represent measurements made in cirrus clouds (shown by the dashed line in Fig. 6).

### 3.1. Quantifying Condensed-Phase HNO<sub>3</sub>

As stated previously,  $\text{HNO}_3|_{\text{front}}$  represents the sum of gas-phase and condensed-phase  $\text{HNO}_3$ , with the condensed-phase component enhanced by the value of  $EF$ . The amount of  $\text{HNO}_3$  condensed on cirrus cloud particles ( $\text{HNO}_3|_{\text{con}}$ ) can therefore be calculated according to equation (1),

$$\text{HNO}_3|_{\text{con}} = \frac{\text{HNO}_3|_{\text{front}} - \text{HNO}_3|_{\text{gas}}}{EF} \quad (1)$$

where  $\text{HNO}_3|_{\text{con}}$  is reported as a gas-phase equivalent volume mixing ratio with a precision of 3 pptv ( $1\sigma$ , 10-s averages). The use of equation (1) in calculating  $\text{HNO}_3|_{\text{con}}$  is illustrated in Fig. 7 for a cirrus cloud encounter by the WB-57F on July 13, 2002. Increases in SAD and IWC during this cloud event are accompanied by an increase in  $\text{HNO}_3|_{\text{front}}$  above the gas-phase value of approximately 0.5 ppbv (Fig. 7a,d,e). Accounting for the particle enhancement factor of approximately 13.7 using equation (1), maximum values of  $\text{HNO}_3|_{\text{con}}$  during this cloud event approached 0.1 ppbv (Fig. 7b,c). It should be noted here that calculated values of  $\text{HNO}_3|_{\text{con}}$  in cirrus clouds are not always consistent with the observed decreases in  $\text{HNO}_3|_{\text{gas}}$  that result from  $\text{HNO}_3$  uptake. Quantitative agreement between  $\text{HNO}_3|_{\text{con}}$  and deficits in  $\text{HNO}_3|_{\text{gas}}$  can only occur if the cloud particles are sampled in the same air mass in which uptake occurred. Due to gravitational settling, however, cirrus particles may sediment into air masses that may be more or less depleted in gas-phase  $\text{HNO}_3$  at the time of sampling.

### 3.2. Cirrus Cloud Particle Measurements

Cirrus cloud particle SAD was derived from measurements provided by both the CAPS and CIN instruments onboard the WB-57F during CRYSTAL-FACE. SAD was derived from the CAPS data by integrating particle size distribution and number density measurements, while bulk measurements of cloud extinction coefficient at 635 nm were used to derive SAD from the CIN data. A comparison between the CIN- and CAPS-derived SADs indicates good agreement between the two instruments for the flights on

July 11, 19 and 21, with SADs derived from the CIN measurements ranging from 23-  
39% higher than the CAPS-derived values on those 3 flight days (Fig. 8). On July 13, the  
CIN measurements were 54% higher than the CAPS values, which may be attributable to  
the sampling of optically thin subvisual cirrus clouds near the tropopause on that day.  
Cloud extinction in these subvisual cirrus is close to the sensitivity threshold of the CIN.  
The observed differences are nonetheless within the combined uncertainties of the two  
instruments on all 4 flight days. The analyses presented here make use of SADs derived  
from the CAPS measurements. Due to the fact that the SADs derived from the CIN  
measurements are 23-54% higher than the CAPS values, the SADs utilized here can be  
considered lower limits.

As stated previously, the value of  $EF$  used in calculating  $\text{HNO}_3|_{\text{con}}$  approaches a  
maximum value of  $U_0/U$  (the ratio of the WB-57F true air speed to the air velocity in the  
sample inlet) at particle sizes greater than approximately  $10 \mu\text{m}$ . SADs calculated from  
the CAPS measurements on the 4 flight days considered here (in cirrus clouds with total  
SADs greater than  $200 \mu\text{m}^2\cdot\text{cm}^{-3}$ ) indicate that  $92\pm 9\%$  of the surface area resides on  
particles larger than  $10 \mu\text{m}$  in diameter. Use of the maximum value of  $EF$  in calculating  
 $\text{HNO}_3|_{\text{con}}$  via equation (1), therefore, is expected to introduce no more than 10%  
uncertainty into the value of  $\text{HNO}_3|_{\text{con}}$ .

The VMD of cirrus cloud particles observed during CRYSTAL-FACE ranged from  
approximately  $3 \mu\text{m}$  up to  $700 \mu\text{m}$ , with most clouds having VMDs greater than  $20 \mu\text{m}$   
(Fig. 9a). The largest particles ( $> 500 \mu\text{m}$ ) were observed primarily in clouds with SADs  
greater than  $10^4 \mu\text{m}^2\cdot\text{cm}^{-3}$ . As expected, IWC shows a strong correlation with SAD (Fig.  
9b). IWCs as high as 1000 ppmv were observed during some cloud events (Fig. 9b). The  
highest values of VMD and IWC were observed from the WB-57F primarily at  
temperatures between 205 K and 215 K during the flights shown in Fig. 9.

## 4. Discussion

### 4.1. $\text{HNO}_3$ Uptake on Cirrus Cloud Particles

2 The coincident observation of cirrus clouds and condensed-phase HNO<sub>3</sub> during  
CRYSTAL-FACE is assumed here to result from the uptake of HNO<sub>3</sub> on the surface of  
cirrus cloud particles. Laboratory studies indicate that the low solubility of HNO<sub>3</sub> in ice  
4 will not allow a significant fraction of HNO<sub>3</sub>|<sub>con</sub> to reside in the bulk of the cirrus  
particles [Sommerfeld *et al*, 1998, Hanson and Ravishankara, 1991]. Furthermore,  
6 *Dominé and Thibert* [1996] have suggested that the high diffusivity of HNO<sub>3</sub> in ice is  
such that HNO<sub>3</sub> trapped in the bulk ice during particle formation will migrate to the  
8 particle surface. We note, however, that the measurements presented here cannot  
distinguish between surface uptake and HNO<sub>3</sub> that may be condensed in the bulk of the  
10 particles. HNO<sub>3</sub> uptake on cirrus cloud particles can be represented in terms of  
molecular coverage, given by the ratio of HNO<sub>3</sub>|<sub>con</sub> to SAD in units of molecules·cm<sup>-2</sup>.  
12 HNO<sub>3</sub> surface coverages observed during CRYSTAL-FACE are shown as a function of  
temperature in Fig. 10, with symbols colored according to  $P(\text{HNO}_3)$  (see legend). Data  
14 shown by triangles at temperatures less than 200 K in Fig.10 represent observations under  
conditions in which nitric acid trihydrate (NAT) is stable, as predicted by ambient  
16 temperature and the ratio of HNO<sub>3</sub>|<sub>gas</sub> to H<sub>2</sub>O vapor [Hanson and Mauersberger, 1988,  
*Gao et al.*, 2003]. It has been proposed that, under conditions in which NAT is stable,  
18 HNO<sub>3</sub> forms NAT clusters or layers on the particle surface which interfere with the  
condensation of H<sub>2</sub>O molecules on the particle surface, and thereby increase the relative  
20 humidity with respect to ice in the cirrus cloud [Gao *et al.*, 2003].

The mean HNO<sub>3</sub> coverage observed during CRYSTAL-FACE was  $1.9 \cdot 10^{13}$   
22 molecules·cm<sup>-2</sup>, with maximum coverages reaching  $1.4 \cdot 10^{14}$  molecules·cm<sup>-2</sup> during a  
few cirrus cloud events (Fig. 10). While the greatest coverages were observed at  
24 temperatures between 205 K and 210 K, mean coverages binned according to  
temperature show no temperature dependence above 200 K (black symbols in Fig. 10).  
26 The average value for measurements between 195 K and 200 K is approximately a factor  
of 3 greater than values above 200 K. Generally higher HNO<sub>3</sub> coverages at lower

temperatures have been observed in field measurements reported by both *Kondo et al.* [2003] and *Ziereis et al.* [2003]. HNO<sub>3</sub> coverages show a minimal dependence on  $P(\text{HNO}_3)$ , with the lowest coverages occurring at  $P(\text{HNO}_3)$  values below  $2.5 \cdot 10^{-8}$  hPa (Fig. 10). A number of laboratory studies have also reported increased HNO<sub>3</sub> coverages with increasing  $P(\text{HNO}_3)$ , albeit at  $P(\text{HNO}_3)$  values substantially higher than those presented here ( $5.0 \cdot 10^{-7}$  -  $3.0 \cdot 10^{-6}$  hPa) [*Hudson et al.*, 2002, *Hynes et al.*, 2002]. These results highlight the need for a comprehensive laboratory study of HNO<sub>3</sub> uptake on ice surfaces at  $P(\text{HNO}_3)$  values below  $2.0 \cdot 10^{-7}$  hPa that are typical of the subtropical UT.

The coverage of HNO<sub>3</sub> on ice, in general, can be modeled or predicted using the kinetics or thermodynamics of the uptake process [*Gao et al.*, 2003, *Hudson et al.*, 2002]. Using laboratory measurements and a semi-empirical equilibrium surface coverage model, *Hudson et al.* [2002] have predicted HNO<sub>3</sub> coverage on ice surfaces as a function of temperature and  $P(\text{HNO}_3)$ . This multilayer Frenkel-Halsey-Hill (FHH) model was fitted to equilibrium HNO<sub>3</sub> coverages observed on vapor-deposited ice films at temperatures between 213 K and 219 K with a  $P(\text{HNO}_3)$  of  $1.1 \cdot 10^{-6}$  hPa. HNO<sub>3</sub> surface coverages predicted by the FHH model are shown as a function of temperature in Fig. 11a, together with the HNO<sub>3</sub> coverages observed in cirrus clouds during CRYSTAL-FACE. The isobaric lines representing the modeled coverages are colored on the same scale as the observed coverages according to the values of  $P(\text{HNO}_3)$  input to the model. Fig 11a indicates better agreement between the modeled and observed HNO<sub>3</sub> coverages at temperatures higher than approximately 205 K, while at lower temperatures the modeled coverages increase to values far greater than those observed at comparable temperatures and  $P(\text{HNO}_3)$  values. The high model coverages below 205 K may result from the fact that the model was fitted to laboratory data at temperatures above 213 K, and the coverages presented here, therefore, are extrapolated to lower temperatures where the uncertainty in the model increases.

A number of studies have described the uptake of HNO<sub>3</sub> on ice surfaces using a

Langmuir surface chemistry model [Tabazdeh *et al.*, 1999, Hynes *et al.*, 2002, Meier *et al.*, 2002]. The Langmuir isotherm predicts the fractional HNO<sub>3</sub> surface coverage ( $\theta$ ) according to equation 2,

$$\theta = \frac{K_{eq}^{1/2} \cdot P(\text{HNO}_3)^{1/2}}{1 + K_{eq}^{1/2} \cdot P(\text{HNO}_3)^{1/2}} \quad (2)$$

where  $K_{eq}$  represents the equilibrium adsorption constant, given by the ratio of the rates of adsorption and desorption ( $k_a/k_d$ ) [Laidler and Meiser, 1982]. The value of  $\theta$  is unity when the HNO<sub>3</sub> surface coverage reaches a complete monolayer ( $1.0 \cdot 10^{15}$  molecules·cm<sup>-2</sup>). We note that the surface density of HNO<sub>3</sub> molecules when forming a complete monolayer is somewhat uncertain, and the density of  $1.0 \cdot 10^{15}$  molecules·cm<sup>-2</sup> stated here should be considered an upper limit [Hudson *et al.*, 2002]. If the HNO<sub>3</sub> surface density is lower than  $1.0 \cdot 10^{15}$  molecules·cm<sup>-2</sup> for a complete monolayer, the resulting fractional surface coverages will be higher than those stated here. Application of the dissociative form of the Langmuir isotherm is supported here by spectroscopic studies of HNO<sub>3</sub> uptake on thin ice films at 211 K, which indicate, by the presence of H<sub>3</sub>O<sup>+</sup> and NO<sub>3</sub><sup>-</sup> ions on the ice surface, that HNO<sub>3</sub> dissociates upon adsorption [Zondlo *et al.*, 1997]. The temperature-dependent equilibrium adsorption constant in equation (2) can be calculated according to equation (3) [Adamson and Gast, 1997],

$$K_{eq} = \frac{100 \cdot N_A \cdot \sigma_0 \cdot \tau_0}{(2\pi \cdot M \cdot R \cdot T)^{1/2}} e^{\left( \frac{-\Delta H_{ads}}{c \cdot R \cdot T} \right)} \text{ hPa}^{-1} \quad (3)$$

where  $N_A$  is Avogadro's number ( $6.02 \cdot 10^{23}$  mol<sup>-1</sup>),  $\sigma_0$  is the area of one adsorption site ( $10^{-19}$  m<sup>2</sup>),  $\tau_0$  is the time constant for adsorbate oscillation perpendicular to the surface ( $10^{-13}$  s),  $M$  is the molecular weight of HNO<sub>3</sub> ( $0.063$  kg·mol<sup>-1</sup>),  $R$  is the ideal gas constant ( $8.314$  J·mol<sup>-1</sup>·K<sup>-1</sup>),  $T$  is temperature (in K),  $c$  is a unit conversion factor ( $2.39 \cdot 10^{-4}$  kcal·J<sup>-1</sup>) and  $\Delta H_{ads}$  is the adsorption enthalpy of HNO<sub>3</sub> on ice (in kcal·mol<sup>-1</sup>).

Using equations (2) and (3), a Langmuir isotherm was fitted to the CRYSTAL-FACE observations of fractional surface coverage and  $P(\text{HNO}_3)$  (Fig. 12). Using the median temperature of 208 K for the observations shown in Fig. 9, the best fit to the experimental data was achieved with a  $\Delta H_{ads}$  of  $-11.0 \text{ kcal}\cdot\text{mol}^{-1}$ , or  $46.0 \text{ kJ}\cdot\text{mol}^{-1}$  (red line in Fig. 12). Note that the data are largely bound by  $\Delta H_{ads}$  values of  $-10.0 \text{ kcal}\cdot\text{mol}^{-1}$  and  $-12.0 \text{ kcal}\cdot\text{mol}^{-1}$ . Also shown in Fig. 12 are Langmuir isotherms at the same temperature for  $\Delta H_{ads}$  values of  $-14.2 \text{ kcal}\cdot\text{mol}^{-1}$  and  $-12.9 \text{ kcal}\cdot\text{mol}^{-1}$  reported by *Tabazadeh et al.* [1998] and *Hynes et al.*, [2002], respectively. Fractional coverages predicted using these previously published values of  $\Delta H_{ads}$  far exceed the coverages observed during CRYSTAL-FACE, indicating these adsorption enthalpies are too high to accurately describe the observations presented here. *Bartels-Rausch et al.* [2002], using a chromatographic technique, have recently reported a  $\Delta H_{ads}$  for  $\text{HNO}_3$  uptake on ice of  $-10.5 \text{ kcal}\cdot\text{mol}^{-1}$  that is in good agreement with the value of  $-11.0 \text{ kcal}\cdot\text{mol}^{-1}$  presented here. We caution that the effective  $\Delta H_{ads}$  reported here is empirically derived from observations in a dynamic system which may or may not be in steady state, and this value, therefore, cannot be considered a fundamental thermodynamic parameter. Nonetheless, the Langmuir formalism, using a  $\Delta H_{ads}$  of  $-11.0 \text{ kcal}\cdot\text{mol}^{-1}$ , effectively describes the CRYSTAL-FACE observations of  $\text{HNO}_3$  uptake on cirrus cloud particles to within a factor of 5 (Fig. 12). It should be noted that the data shown in Fig. 12 span a temperature range from 197 K to 218 K, and that the Langmuir isotherms were fitted at the median temperature of 208 K. Use of a single temperature in fitting the isotherms is supported by the results of *Hynes et al.* [2002], who reported a variation of less than 2% between values of  $\Delta H_{ads}$  derived from laboratory measurements at 218 K and 228 K.

Having derived an effective value of  $\Delta H_{ads}$  for  $\text{HNO}_3$  adsorption on cirrus cloud particles in the UT,  $\text{HNO}_3$  coverages predicted by the Langmuir surface chemistry model (as a function of temperature) can be compared to the CRYSTAL-FACE observations (Fig. 11b). As in Fig. 11a, the isobaric lines are colored on the same scale as the

observed coverages. The calculated coverages shown in Fig. 11b indicate that the model does not adequately describe the considerable variability in the observed coverages at a given temperature and  $P(\text{HNO}_3)$ . Nonetheless, when using the empirically derived  $\Delta H_{ads}$  of  $-11.0 \text{ kcal}\cdot\text{mol}^{-1}$ , the Langmuir model is capable of predicting the observed coverages within a factor of 5 or better. The variability in the observed coverages, and the less than perfect agreement with the uptake models, can be explained, in part, if the adsorbed  $\text{HNO}_3$  is not in equilibrium with  $\text{HNO}_3$  in the gas phase. Previous field studies have also shown  $\text{HNO}_3$  surface coverages to be highly variable throughout the temperature and  $P(\text{HNO}_3)$  ranges observed [Kondo *et al.*, 2002, Ziereis *et al.*, 2003].

#### 4.2. $\text{HNO}_3$ Partitioning in Cirrus Clouds

The fraction of total  $\text{HNO}_3$  present on cirrus cloud particles was observed to increase with SAD during CRYSTAL-FACE (Fig. 13). The mean value of  $\text{HNO}_3$  partitioned in the condensed phase at SADs greater than  $200 \mu\text{m}^2\cdot\text{cm}^{-3}$  was 16%. Up to 100% of the total  $\text{HNO}_3$  was partitioned on ice particles during some cirrus cloud encounters, at SADs between 350 and  $4.2\cdot 10^4 \mu\text{m}^2\cdot\text{cm}^{-3}$  and temperatures between 201 K and 213 K.

Measurements reported by Ziereis *et al.* [2003] in midlatitude cirrus clouds reveal a similar relationship between condensed-phase  $\text{NO}_y$  partitioning and SAD, although maximum reported values of condensed-phase  $\text{NO}_y$  partitioned in cirrus clouds did not exceed 50% of the total observed  $\text{NO}_y$ . Measurements of  $\text{NO}_y$  uptake in a mountain wave cirrus cloud reported by Weinheimer *et al.* [1998] indicate complete uptake of  $\text{HNO}_3$ , provided that the ambient  $\text{HNO}_3/\text{NO}_y$  ratio in the cloud was 0.1-0.2. Gas-phase  $\text{HNO}_3$  was not measured in either of these previous studies, making an accurate assessment of the fraction of  $\text{HNO}_3$  remaining in the gas phase after uptake difficult.

Krämer *et al.* [2003] have recently studied the partitioning of  $\text{HNO}_3$  in Arctic cirrus clouds, and have modeled the role of  $\text{HNO}_3$  uptake by interstitial  $\text{HNO}_3\text{-H}_2\text{SO}_4\text{-H}_2\text{O}$  ternary solution aerosols in partitioning. This study concluded that some fraction of the total  $\text{HNO}_3$  in Arctic cirrus clouds must remain in the gas phase, with the remainder

partitioned predominately in interstitial aerosols at temperatures less than 205 K when  
2 SADs are low, and on cirrus cloud particles at higher SADs. Measurements in  
subtropical cirrus clouds reported here, however, indicate that up to 100% of the total  
4  $\text{HNO}_3$  can be partitioned in cirrus ice particles both at low temperatures and low SADs.  
Furthermore, we see no evidence of significant uptake of  $\text{HNO}_3$  in ternary solution  
6 aerosols outside of clouds in the subtropical UT during the flights considered in this  
study. There is evidence, however, of  $\text{HNO}_3$  uptake by ternary solution aerosols in the  
8 near absence of cirrus ice particles on at least one other CRYSTAL-FACE flight (July 9,  
2002) [Weinheimer *et al.*, 2002]. We also note that  $\text{HNO}_3$  may be contained in a ternary  
10 solution on the surface of the cirrus ice particles.

### 4.3. $\text{HNO}_3$ and $\text{HNO}_3/\text{NO}_y$ in the Cloud-Free Upper Troposphere and Lower 12 Stratosphere

Measurements in the cloud-free subtropical UT during CRYSTAL-FACE indicate  
14 that the gas-phase  $\text{HNO}_3/\text{NO}_y$  ratio is highly variable, ranging from zero to  
approximately 0.5 (colored symbols in Fig. 14a). The  $\text{HNO}_3/\text{NO}_y$  ratio is generally  
16 higher and also variable in the subtropical lower stratosphere (LS), with values observed  
between 0.05 and 1 (black symbols in Fig. 14a).  $\text{HNO}_3$  is expected to be the predominate  
18  $\text{NO}_y$  species in the LS away from the tropopause region [Neuman *et al.*, 2001]. The  
lower  $\text{HNO}_3/\text{NO}_y$  ratios ( $< 0.3$ ) observed in the UT are affected by low observed values  
20 of  $\text{HNO}_3$ , due to  $\text{HNO}_3$  removal by uptake and sedimentation by cloud particles in cirrus  
processed air masses (yellow symbols in Fig. 14b), or from elevated levels of  $\text{NO}_y$  due to  
22 NO production from lightning strikes (purple symbols in Fig. 14b). Previously measured  
values of the  $\text{HNO}_3/\text{NO}_y$  ratio in the midlatitude UT over the continental United States  
24 were also highly variable and ranged from approximately 0.1 to 0.5 [Neuman *et al.*,  
2001]. The large range and variability of  $\text{HNO}_3/\text{NO}_y$  ratios observed in the UT during  
26 CRYSTAL-FACE highlights the value in measuring gas-phase  $\text{HNO}_3$  when assessing  
 $\text{HNO}_3$  uptake on cirrus cloud particles, over deriving gas-phase  $\text{HNO}_3$  from measured

NO<sub>y</sub> and a constant assumed HNO<sub>3</sub>/NO<sub>y</sub> ratio.

2 A number of cirrus clouds observed in the subtropical UT during CRYSTAL-FACE  
had VMDs between 200 μm and 700 μm. Terminal fall velocities for cirrus ice particles  
4 in this size range are 1 m·s<sup>-1</sup> to 10 m·s<sup>-1</sup> (Fig. 9a) [Meier and Hendricks, 2002]. With  
16% of the total HNO<sub>3</sub> in cirrus clouds adsorbed on ice particles, the gravitational  
6 redistribution of a significant fraction of the total HNO<sub>3</sub> in these clouds can therefore  
occur on a timescale of minutes to hours. Cirrus clouds with up to 100% of the total  
8 HNO<sub>3</sub> partitioned in the condensed phase have even greater potential to redistribute  
HNO<sub>3</sub> in the UT.

## 10 **5. Conclusions and Implications**

A number of cirrus cloud encounters in the UT by the NASA WB-57F during  
12 CRYSTAL-FACE were accompanied by the observation of condensed-phase HNO<sub>3</sub>.  
Maximum levels of condensed-phase HNO<sub>3</sub> exceeded the gas-phase equivalent of 0.8  
14 ppbv during some cirrus events. A mean HNO<sub>3</sub> surface coverage of  $1.9 \cdot 10^{13}$   
molecules·cm<sup>-2</sup> was observed on the flights of July 11, 13, 19 and 21, 2002, with  
16 maximum surface coverages reaching as high as  $1.4 \cdot 10^{14}$  molecules·cm<sup>-2</sup> during a few  
cirrus cloud encounters. Molecular coverages predicted using a Langmuir surface  
18 chemistry model agree with the observed coverages to within a factor of 5 or better when  
using an empirically derived  $\Delta H_{ads}$  of  $-11.0$  kcal·mol<sup>-1</sup>. The mean percentage of total  
20 HNO<sub>3</sub> condensed on cirrus cloud particles was 16%, with up to 100% of the HNO<sub>3</sub>  
partitioned in the condensed phase in a number of cirrus clouds. The fraction of total  
22 HNO<sub>3</sub> in the condensed phase was found to increase strongly with SAD. Based on the  
large diameters of cloud particles containing HNO<sub>3</sub> observed during CRYSTAL-FACE,  
24 the redistribution of HNO<sub>3</sub> in the UT will be very effective in some cloud systems. The  
interpretation of future observations of HNO<sub>3</sub> uptake on cirrus particles will be improved  
26 by a knowledge of the individual history of the air parcels in which the cirrus clouds are  
formed [Kärcher, 2003] and laboratory studies of HNO<sub>3</sub> uptake at low gas-phase

abundances ( $P(\text{HNO}_3) < 2.0 \cdot 10^{-7}$  hPa) and low temperatures (195 K – 220 K).

## 2 **Acknowledgements**

The authors wish to thank the air and ground crews of the NASA WB-57F aircraft.

4 Helpful discussions with J.P.D. Abbatt, E.R. Lovejoy and H. Ziereis are also appreciated.

This work was partially supported by the National Aeronautics and Space Administration

6 Upper Atmospheric Research Program and Radiation Science Program. Work done by

MJM at the Jet Propulsion Laboratory, California Institute of Technology, was carried

8 out under contract with the National Aeronautics and Space Administration.

## References

2  
4  
6  
8  
10  
12  
14  
16  
18  
20  
22  
24  
26  
28  
30  
32  
34  
36  
38  
40  
42

Abbatt, J.P.D., Interaction of HNO<sub>3</sub> with water-ice surfaces at temperatures of the free troposphere, *Geophys. Res. Lett.*, 24(12), 1479-1482, 1997.

Adamson, A.W. and A.P. Gast, *Physical Chemistry of Surfaces*, 6th Ed., John Wiley & Sons, New York, 1997.

Albritton, D.L., et al., Technical Summary of the Working Group I Report, in *Climate Change 2001: The Scientific Basis. Contribution of Working Group I to the Third Assessment Report of the Intergovernmental Panel on Climate Change*, edited by J.T. Houghton et al., pp. 21-83, Cambridge University Press, Cambridge and New York, 2001.

Arora, O.P., et al., Uptake of nitric acid by sub-micron-sized ice particles, *Geophys. Res. Lett.*, 26(24), 3621-3624, 1999.

Bartels-Rausch, T., et al., The adsorption enthalpy of nitrogen oxides on crystalline ice, *Atmos. Chem. Phys.* 2, 235-247, 2002.

Baumgardner, D., et al., The cloud, aerosol and precipitation spectrometer: a new instrument for cloud investigations, *Atmos. Res.*, 59-60, 251-264, 2001.

Denning, R.F., S.L. Guidero, G.S. Parks, B.L. Gary, Instrument description of the Airborne Microwave Temperature Profiler, *J. Geophys. Res.*, 94, 16,757-16,765, 1989.

Dominé, F. and E. Thibert, Mechanism of incorporation of trace gases in ice grown from the gas phase, *Geophys. Res. Lett.*, 23(24), 3627-3630, 1996.

Gao, R.S., et al., Evidence that Ambient Nitric Acid Increases Relative Humidity in Low-Temperature Cirrus Clouds, In press. *Science*, 2003.

Gerber, H., Y. Takano, T.J. Garrett, and P.V. Hobbs, Nephelometer Measurements of the Asymmetry Parameter, Volume Extinction Coefficient, and Backscatter Ratio in Arctic Clouds, *J. Atmos. Sci.* 57, 3021-3034, 2000.

Hanson, D. and K. Mauersberger, Laboratory studies of the nitric acid trihydrate: implications for the south polar stratosphere, *Geophys. Res. Lett.*, 15(8), 855-858, 1988.

Hanson, D.R. and A.R. Ravishankara, The reaction probabilities of ClONO<sub>2</sub> and N<sub>2</sub>O<sub>5</sub> on polar stratospheric cloud materials, *J. Geophys. Res.*, 96(3), 5081-5090, 1991.

- 2 Heymsfield, A.J. and G.M. McFarquhar, Mid-latitude and Tropical Cirrus: Microphysical  
Properties, in *Cirrus*, edited by D.K. Lynch, K. Sassen, D. O’C. Starr, and G.  
4 Stephens, pp. 78-101, Oxford University Press, Oxford, 2002.
- 6 Hudson, P.K., et al., Uptake of Nitric Acid on Ice at Tropospheric Temperatures:  
Implications for Cirrus Clouds, *J. Phys. Chem. A*, *106*, 9874-9882, 2002.
- 8 Hynes, R.G., M.A. Fernandez, and R.A. Cox, Uptake of HNO<sub>3</sub> on water-ice and  
coadsorption of HNO<sub>3</sub> and HCl in the temperature range 210-235 K, *J. Geophys. Res.*,  
10 *107*(D24), 4797, doi:10.1029/2001JC001557, 2002.
- 12 Jaeglé, L., et al., Sources of HO<sub>x</sub> and production of ozone in the upper troposphere over  
the United States, *Geophys. Res. Lett.*, *25*(10), 1709-1712, 1998.
- 14 Jin, Y., W.B. Rossow, D.P. Wylie, Comparison of the Climatologies of High-Level  
16 Clouds from HIRS and ISCCP, *J. Climate.*, *9*, 2850-2879, 1996.
- 18 Kärcher, B., Properties of subvisible cirrus clouds formed by homogeneous freezing,  
*Atmos. Chem. Phys.*, *2*, 161-170, 2002.
- 20 Kärcher, B., Simulating gas-aerosol-cirrus interactions: Process-oriented microphysical  
22 model and applications, *Atmos. Chem. Phys.*, *3*, 1645-1664, 2003.
- 24 Kondo, Y., et al., Uptake of reactive nitrogen on cirrus cloud particles in the upper  
troposphere and lowermost stratosphere, *Geophys. Res. Lett.*, *30*(4), 1154,  
26 doi:10.1029/2002GL016539, 2003.
- 28 Krämer, M., et al., Nitric acid partitioning in cirrus clouds: a synopsis based on field,  
laboratory and model studies, *Atmos. Chem. Phys. Discuss.* *3*, 413-443, 2003.
- 30 Lacis, A.A., D.J. Wuebbles, and J.A. Logan, Radiative Forcing of Climate by Changes in  
32 the Vertical Distribution of Ozone, *J. Geophys. Res.*, *95*(D7), 9971-9982, 1990.
- 34 Laidler, K.J. and J.H. Meiser, *Physical Chemistry*, Benjamin Cummings, Menlo Park,  
1982.
- 36 Lawrence, M.G. and P.J. Crutzen, The impact of cloud particle gravitational settling on  
38 soluble trace gas distributions, *Tellus*, *50B*, 263-289, 1998.
- 40 Liao, X., W.B. Rossow, and D. Rind, Comparison between SAGE II and ISCCP high-  
level clouds: 1. Global and zonal mean cloud amounts, *J. Geophys. Res.*, *100*(D1),  
42 1121-1135, 1995.

- 2 Liou, K.-N., Influence of Cirrus Clouds on Weather and Climate Processes: A Global  
Perspective, *Mon. Wea. Rev.* 114, 1167-1199, 1986.
- 4 Lynch, D.K., Cirrus History and Definition, in *Cirrus*, edited by D.K. Lynch, K. Sassen,  
D. O’C. Starr, and G. Stephens, pp. 3-10, Oxford University Press, Oxford, 2002.
- 6 Meier, A. and J. Hendricks, Model studies on the sensitivity of upper tropospheric  
8 chemistry to heterogeneous uptake of HNO<sub>3</sub> on cirrus ice particles, *J. Geophys. Res.*,  
107(D23), 4696, doi:10.1029/2001JD000735, 2002.
- 10 Meilinger, S.K., et al., HNO<sub>3</sub> Partitioning in Cirrus Clouds, *Geophys. Res. Lett.* 26(14),  
12 2207-2210, 1999.
- 14 Neuman, J.A. et al., Study of Inlet Materials for Sampling Atmospheric Nitric Acid, 33,  
1133-1136, 1999.
- 16 Neuman, J.A. et al., A fast-response chemical ionization mass spectrometer for *in situ*  
18 measurements of HNO<sub>3</sub> in the upper troposphere and lower stratosphere, *Rev. Sci.*  
*Instrum.*, 71(10), 3886-3892, 2000.
- 20 Neuman, J.A., et al., In situ measurements of HNO<sub>3</sub>, NO<sub>y</sub>, NO, and O<sub>3</sub> in the lower  
22 stratosphere and upper troposphere, *Atmos. Environ.*, 35, 5789-5797, 2001.
- 24 Northway, M.J., et al., An analysis of large HNO<sub>3</sub>-containing particles sampled in the  
Arctic stratosphere during the winter of 1999/2000, *J. Geophys. Res.*, 107(D20), 8298,  
26 doi:10.1029/2001JD001079, 2002.
- 28 Sassen, K., Cirrus Clouds: A Modern Perspective, in *Cirrus*, edited by D.K. Lynch, K.  
Sassen, D. O’C. Starr, and G. Stephens, pp. 11-40, Oxford University Press, Oxford,  
30 2002.
- 32 Scott, S.G., T.P. Bui, K.R. Chan, and S.W. Bowen, The meteorological measurement  
system on the NASA ER-2 aircraft, *J. Atmos. Oceanic Technol.*, 7, 525-540, 1990.
- 34 Sommerfeld, R.A., C.A. Knight and S.K. Laird, Diffusion of HNO<sub>3</sub> in ice, *Geophys. Res.*  
36 *Lett.*, 25(6), 935-938, 1998.
- 38 Tabazadeh, A., O.B. Toon, E.J. Jensen, A surface chemistry model for nonreactive trace  
gas adsorption on ice: Implications for nitric acid scavenging by cirrus, *Geophys. Res.*  
40 *Lett.*, 26(14), 2211-2214, 1999.

- 2 Vincent, J.H., et al., On the aspiration characteristics of large-diameter thin-walled  
aerosol sampling probes at yaw orientations with respect to the wind, *J. Aerosol Sci.*  
4 *17*(2), 211-224, 1986.
- 6 Wang, P.-H., et al., A 6-year climatology of cloud occurrence frequency from  
Stratospheric Aerosol and Gas Experiment II observations (1985-1990), *J. Geophys.*  
8 *Res.*, *101*(D23), 29407-29,429, 1996.
- 10 Weinheimer, A.J. et al., Manuscript in preparation. 2004.
- 12 Weinheimer, A.J., et al., Uptake of NO<sub>y</sub> on wave-cloud ice particles, *Geophys. Res. Lett.*,  
*25*(10), 1725-1728, 1998.
- 14 Weinstock, E.M., et al., New fast-response photofragment fluorescence hygrometer for  
use on the NASA ER-2 and the Perseus remotely piloted aircraft, *Rev. Sci. Instrum.*,  
16 *65*(11), 3544-3554, 1994.
- 18 Weinstock, E.M. et al., Manuscript in preparation. 2004.
- 20 Wylie, D.P., and Menzel, W.P., Eight Years of High Cloud Statistics Using HIRS, *J.*  
*Climate*, *12*, 170-184, 1999.
- 22 Ziereis, H. et al., Uptake of reactive nitrogen on cirrus cloud particles during INCA,  
24 Submitted to *Geophys. Res. Lett.*
- 26 Zondlo, M.A., S.B. Barone, and M.A. Tolbert, Uptake of HNO<sub>3</sub> on ice under upper  
tropospheric conditions, *Geophys. Res. Lett.*, *24*(11), 1391-1394, 1997.

## Figure Captions

2

4 **Figure 1.** Schematic diagram of the NOAA CIMS inlet pylon. Labeled components are  
6 as follows: (a) front channel inlet, (b) bottom channel inlet, (c) zero gas addition, (d)  
8 calibration gas addition, (e) reagent gas carrier addition, (f) reagent gas addition, (g)  
10 HNO<sub>3</sub> permeation cell (calibration standard), (h) flow control valve motor, (i) flow  
12 control valve body, (j) flow tube, (k) ion source, (l) flow straightener. For clarity,  
14 complete components are shown only for the front channel. Inlet lines are constructed of  
Teflon™ tubing (6.4 mm outside diameter, 4.0 mm inside diameter), heated to  
temperatures of 40° C (bottom channel inlet) and 48° C (front channel inlet) to avoid wall  
losses. The higher temperature of the front inlet ensures that ice particles entering the  
inlet evaporate upon impaction with the tubing wall. The operating principles of the  
NOAA CIMS instrument have been described in detail by *Neuman et al.* [2000].

14

16 **Figure 2.** Time series measurements of the HNO<sub>3</sub> mixing ratio observed from the front  
18 and bottom CIMS channels (HNO<sub>3</sub>|<sub>front</sub> and HNO<sub>3</sub>|<sub>gas</sub>, respectively,) on the flight of July  
20 11, 2002. Note that values of HNO<sub>3</sub>|<sub>front</sub> do not include a correction for particle  
22 oversampling in the front channel inlet. Discontinuities in the time series result from  
CIMS instrument calibrations and other housekeeping procedures. Also shown are SAD,  
IWC, water vapor, relative humidity (with respect to ice), and ambient temperature and  
pressure. All data are represented as 10-s averages. Minor divisions on the horizontal  
scale represent 15 minutes (or approximately 150 km) of flight.

24

26 **Figure 3.** Same as Fig. 2, for the flight on July 13, 2002. Purple bars in panel (b)  
28 represent 3 flight segments in which cirrus clouds formed in the contrail of the WB-57F  
30 were observed. The inset in panel (a) shows 1-s averages of HNO<sub>3</sub>|<sub>front</sub> and HNO<sub>3</sub>|<sub>gas</sub>  
during the first contrail intercept. The purple bar in the inset represents the same time  
period as the first purple bar in panel (b). The vertical scale on the inset panel is 0 to 1  
ppbv. Measurements of HNO<sub>3</sub>|<sub>front</sub> and HNO<sub>3</sub>|<sub>gas</sub> are incomplete during the second and  
third contrail intercepts due to instrument housekeeping procedures.

32

34 **Figure 4.** Same as Fig. 2, for the flight on July 19, 2002. Purple bars in panel (b)  
36 represent 2 flight segments in which cirrus clouds formed in the contrail of the WB-57F  
38 were observed. The insets in panel (a) shows 1-s averages of HNO<sub>3</sub>|<sub>front</sub> and HNO<sub>3</sub>|<sub>gas</sub>  
during the two contrail intercepts. The purple bars in the first and second insets represent  
the same time periods as the first and second purple bars in panel (b). The vertical scale  
on the inset panels is 0 to 0.5 ppbv.

38

40 **Figure 5.** Same as Fig. 2, for the flight on July 21, 2002.

40

42 **Figure 6.** (HNO<sub>3</sub>|<sub>front</sub> - HNO<sub>3</sub>|<sub>gas</sub>) vs. SAD for the flights of July 11, 13, 19 and 21,  
2002. Values of (HNO<sub>3</sub>|<sub>front</sub> - HNO<sub>3</sub>|<sub>gas</sub>) are proportional, but not equal to condensed-  
phase HNO<sub>3</sub> (HNO<sub>3</sub>|<sub>con</sub>) because they do not include a correction for particle

oversampling in the front channel inlet. Red circles represent 10-s averages and black squares represent mean values of the 10-s data grouped into deciles. Vertical bars represent the standard deviation about the mean value in each decile, and horizontal bars indicate the upper and lower boundaries of each decile. Note that the vertical axis is shown with a logarithmic scale at values greater than 2.5. The dashed vertical line at the SAD of  $200 \mu\text{m}^2\cdot\text{cm}^{-3}$  represents the lower limit chosen here to represent measurements made in cirrus clouds.

**Figure 7.** Calculation of  $\text{HNO}_3|_{\text{con}}$  for a cirrus cloud encounter by the NASA WB-57F on July 13, 2002, showing  $\text{HNO}_3|_{\text{front}}$  and  $\text{HNO}_3|_{\text{gas}}$  (panel a),  $EF$  (panel b),  $\text{HNO}_3|_{\text{con}}$  (panel c), SAD (panel d) and IWC (panel e). All data are shown as 10-s averages. The horizontal axis spans approximately 16 minutes and 180 km of flight.

**Figure 8.** Comparison of CIN- and CAPS-derived SAD measured during the flights of July 11, 13, 19 and 21, 2002. Data at SADs less than  $3 \mu\text{m}^2\cdot\text{cm}^{-3}$  are expanded in the inset. All data are shown as 10-s averages. Lines represent a least-squares fit to the data for each flight date. The slope of the linear fit (constrained through the origin) is shown for each flight date in the figure legend.

**Figure 9.** Panel (a). Volume-weighted mean diameter of cirrus cloud particles vs. SAD measured during the flights on July 11, 13, 19 and 21, 2002. Only data at SADs greater than  $200 \mu\text{m}^2\cdot\text{cm}^{-3}$  are shown. Data are colored according to ambient temperature. The black line represents the terminal fall velocity for ice particles in the upper troposphere, calculated according to *Meier and Hendricks* [2002]. Panel (b). IWC (represented as a gas-phase equivalent volume mixing ratio) vs. SAD. At 130 hPa and 200 K, an IWC of 100 ppmv is equivalent to an ice water concentration of  $14 \text{ mg}\cdot\text{m}^{-3}$ . Other details same as panel (a).

**Figure 10.**  $\text{HNO}_3$  coverage vs. temperature for measurements made in cirrus clouds at SADs greater than  $200 \mu\text{m}^2\cdot\text{cm}^{-3}$  on July 11, 13, 19 and 21, 2002. Symbols are colored according to  $P(\text{HNO}_3)$ . Triangles at temperatures less than 200 K indicate measurements made under conditions in which NAT is stable. Mean values of  $\text{HNO}_3$  coverage are plotted at the mean of 5 K temperature bins from 195 K to 220 K (black squares). Error bars represent the standard deviation in each temperature bin. Negative values of  $\text{HNO}_3$  coverage are included in the calculation of the mean values. The dashed line at  $1.9\cdot 10^{13}$  molecules $\cdot\text{cm}^{-2}$  represents the mean  $\text{HNO}_3$  coverage observed during CRYSTAL-FACE. A complete  $\text{HNO}_3$  monolayer is formed when the coverage reaches  $1.0\cdot 10^{15}$  molecules $\cdot\text{cm}^{-2}$ .

**Figure 11.**  $\text{HNO}_3$  coverage vs. temperature for measurements made in cirrus clouds at SADs greater than  $200 \mu\text{m}^2\cdot\text{cm}^{-3}$  on July 11, 13, 19 and 21, 2002. Symbols are colored according to  $P(\text{HNO}_3)$ . Triangles at temperatures less than 200 K indicate measurements made under conditions in which NAT is stable. Data are represented as 10-s averages.

2 Panel (a). Lines are isobars representing HNO<sub>3</sub> coverages calculated by the FHH HNO<sub>3</sub>  
uptake model [Hudson *et al.*, 2002] and are colored according to the same temperature  
4 scale as the observed coverages (see legend). Panel (b). Same as panel (a), except the  
isobars represent HNO<sub>3</sub> coverages calculated by the Langmuir surface chemistry model.

6 **Figure 12.** Fractional HNO<sub>3</sub> surface coverage ( $\theta$ ) vs.  $P(\text{HNO}_3)$  measured during the  
flights of July 11, 13, 19 and 21, 2002. Colored lines are isotherms fitted according to  
8 equations (2) and (3) (see text) with values of  $\Delta H_{ads}$  shown in the legend and the median  
observed temperature of 208 K. All data are represented as 10-s averages for  
10 measurements made at SADs greater than  $200 \mu\text{m}^2\cdot\text{cm}^{-3}$ .

12 **Figure 13.** Fraction of total HNO<sub>3</sub> in the condensed phase vs. SAD measured during the  
flights of July 11, 13, 19 and 21, 2002. Data are represented as 10-s averages for  
14 measurements made at SADs greater than  $200 \mu\text{m}^2\cdot\text{cm}^{-3}$  and are colored according to  
temperature. Black squares represent mean values of the 10-s data grouped into quintiles.  
16 Vertical bars represent the standard deviation about the mean value in each quintile and  
horizontal bars represent the upper and lower boundaries of each quintile. Values of  
condensed-phase partitioning greater than 100% occur when zero or near-zero HNO<sub>3|gas</sub>  
18 abundances are measured as negative values. The dashed line at 16% represents the  
mean value of HNO<sub>3</sub> partitioned in the condensed phase during CRYSTAL-FACE.  
20

22 **Figure 14.** Panel (a). Vertical profile of the gas-phase HNO<sub>3</sub>/NO<sub>y</sub> ratio observed in  
cloud free air (SADs less than  $20 \mu\text{m}^2\cdot\text{cm}^{-3}$ ) during the flights of July 11, 13, 19 and 21,  
24 2002. Tropospheric measurements (according to the Microwave Temperature Profiler)  
are colored according to measured NO. Stratospheric measurements are shown in black.  
26 Panel (b). Vertical profile of HNO<sub>3|gas</sub>. Other details same as panel (a).

**Table 1.** Measurement details.

Measurement	Institution	Precision <sup>a</sup>	Accuracy	Reference.
HNO <sub>3</sub>	NOAA Aeronomy Lab	30 pptv, 10 pptv <sup>b</sup>	±20%	<i>Neuman et al., 2002</i>
SAD - CAPS	Univ. Nacional Autonoma de Mexico	-	±50%	<i>Baumgardner et al., 2002</i>
SAD - CIN	University of Utah	-	±15%	<i>Gerber et al., 2000</i>
IWC	Harvard University	0.7 ppmv	±17%	<i>Weinstock et al., 2004</i>
Water Vapor	Harvard University	0.5 ppmv	±5%	<i>Weinstock et al., 1994</i>
NO	NCAR	5 pptv	±6%	<i>Weinheimer et al., 2004</i>
NO <sub>y</sub>	NCAR	8 pptv	±12%	<i>Weinheimer et al., 2004</i>
Temperature	NASA Ames	0.01 K	±0.3 K	<i>Scott et al., 1990</i>
Pressure	NASA Ames	0.1 hPa	±0.3 hPa	<i>Scott et al., 1990</i>
True Air Speed	NASA Ames	0.1 m·s <sup>-1</sup>	±1 m·s <sup>-1</sup>	<i>Scott et al., 1990</i>

<sup>a</sup> Precision values are reported for 10-s averages

<sup>b</sup> 10 pptv is the precision for condensed-phase HNO<sub>3</sub>.

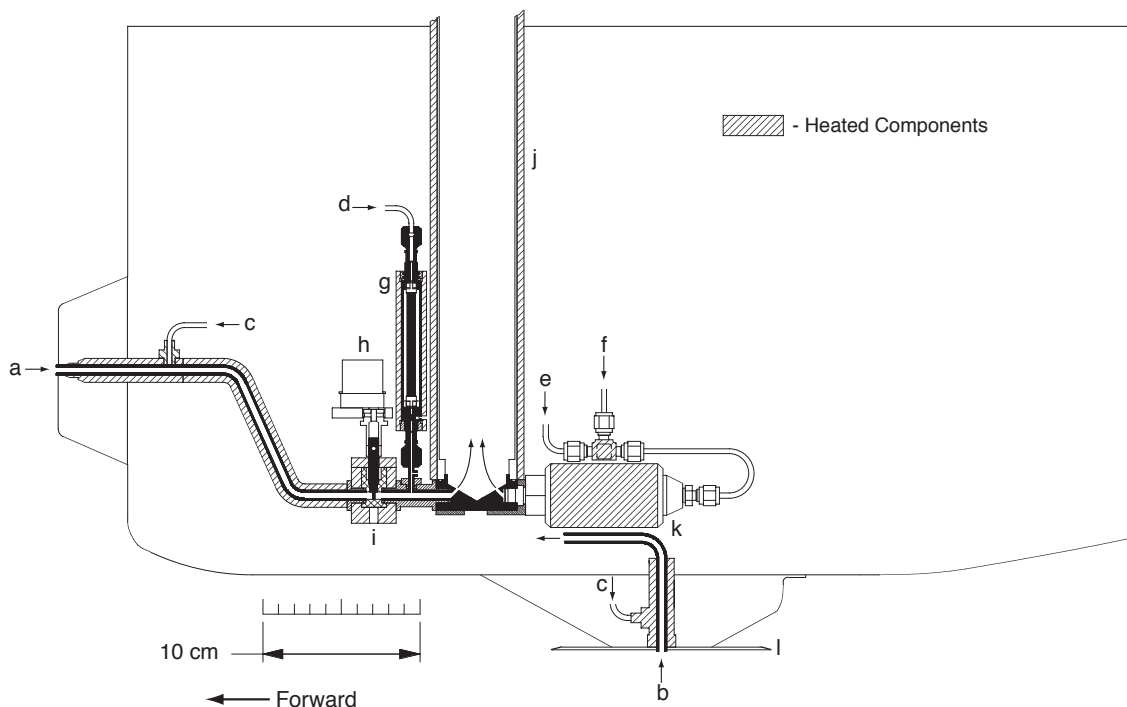


Fig. 1 Popp et al.

**Figure 1.** Schematic diagram of the NOAA CIMS inlet pylon. Labeled components are as follows: (a) front channel inlet, (b) bottom channel inlet, (c) zero gas addition, (d) calibration gas addition, (e) reagent gas carrier addition, (f) reagent gas addition, (g)  $\text{HNO}_3$  permeation cell (calibration standard), (h) flow control valve motor, (i) flow control valve body, (j) flow tube, (k) ion source, (l) flow straightener. For clarity, complete components are shown only for the front channel. Inlet lines are constructed of Teflon™ tubing (6.4 mm outside diameter, 4.0 mm inside diameter), heated to temperatures of 40° C (bottom channel inlet) and 48° C (front channel inlet) to avoid wall losses. The higher temperature of the front inlet ensures that ice particles entering the inlet evaporate upon impactation with the tubing wall. The operating principles of the NOAA CIMS instrument have been described in detail by *Neuman et al.* [2000].

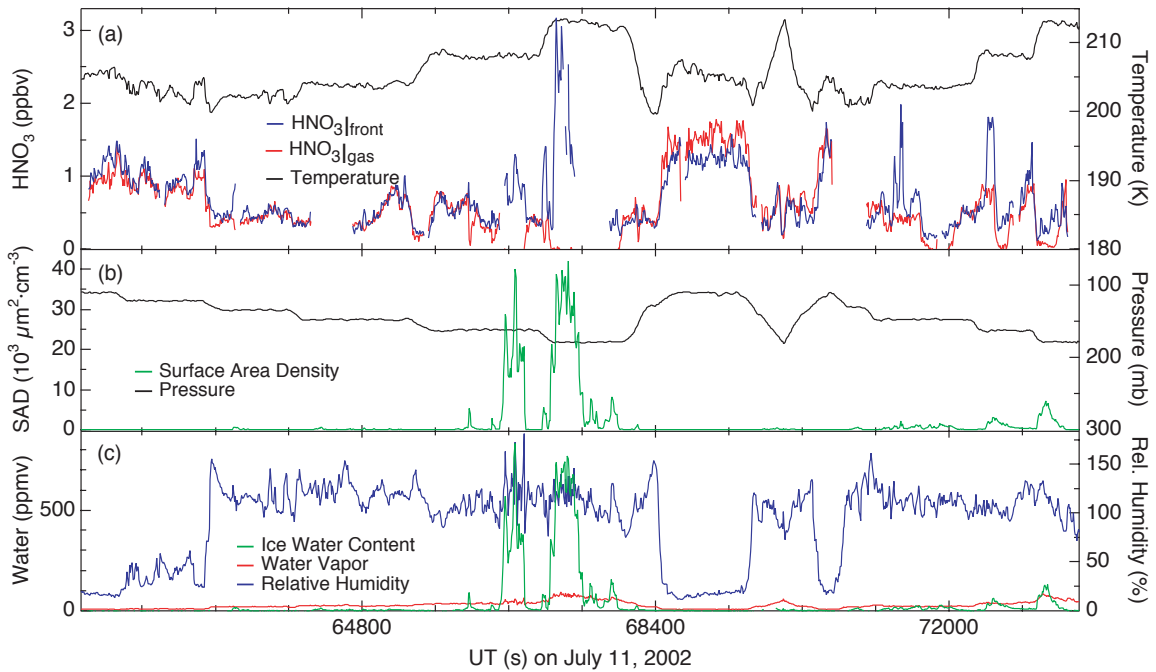


Fig. 2 Popp et al.

**Figure 2.** Time series measurements of the HNO<sub>3</sub> mixing ratio observed from the front and bottom CIMS channels (HNO<sub>3</sub>|<sub>front</sub> and HNO<sub>3</sub>|<sub>gas</sub>, respectively,) on the flight of July 11, 2002. Note that values of HNO<sub>3</sub>|<sub>front</sub> do not include a correction for particle oversampling in the front channel inlet. Discontinuities in the time series result from CIMS instrument calibrations and other housekeeping procedures. Also shown are SAD, IWC, water vapor, relative humidity (with respect to ice), and ambient temperature and pressure. All data are represented as 10-s averages. Minor divisions on the horizontal scale represent 15 minutes (or approximately 150 km) of flight.

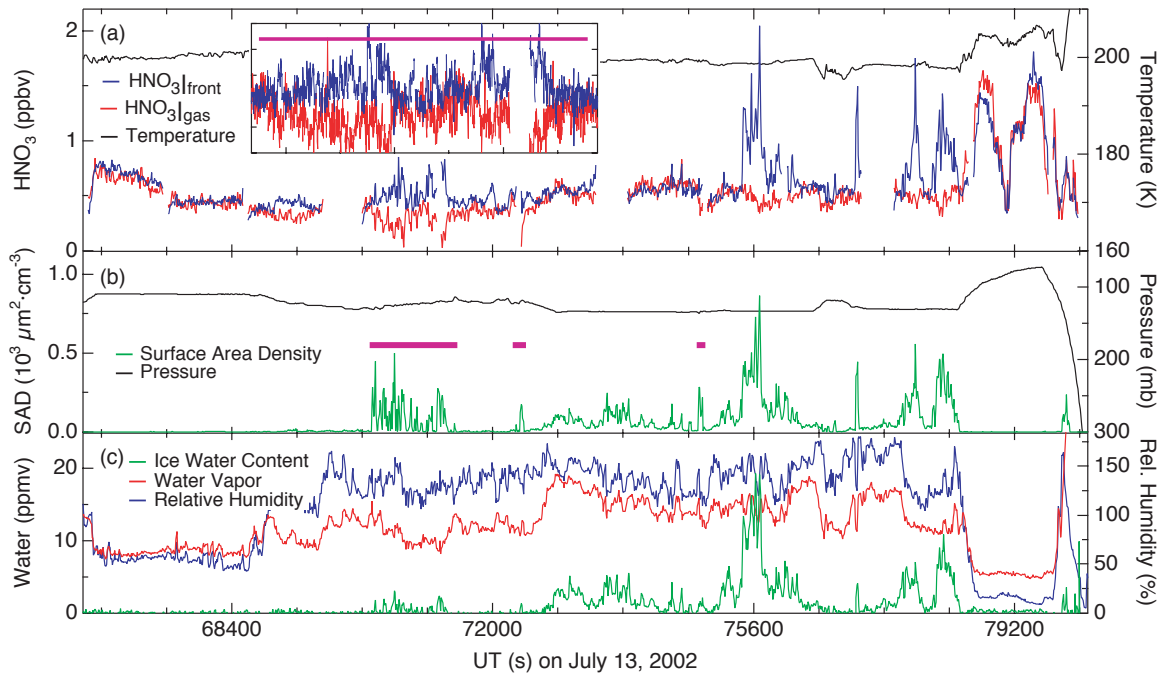


Fig. 3 Popp et al.

**Figure 3.** Same as Fig. 2, for the flight on July 13, 2002. Purple bars in panel (b) represent 3 flight segments in which cirrus clouds formed in the contrail of the WB-57F were observed. The inset in panel (a) shows 1-s averages of  $\text{HNO}_3|_{\text{front}}$  and  $\text{HNO}_3|_{\text{gas}}$  during the first contrail intercept. The purple bar in the inset represents the same time period as the first purple bar in panel (b). The vertical scale on the inset panel is 0 to 1 ppbv. Measurements of  $\text{HNO}_3|_{\text{front}}$  and  $\text{HNO}_3|_{\text{gas}}$  are incomplete during the second and third contrail intercepts due to instrument housekeeping procedures.

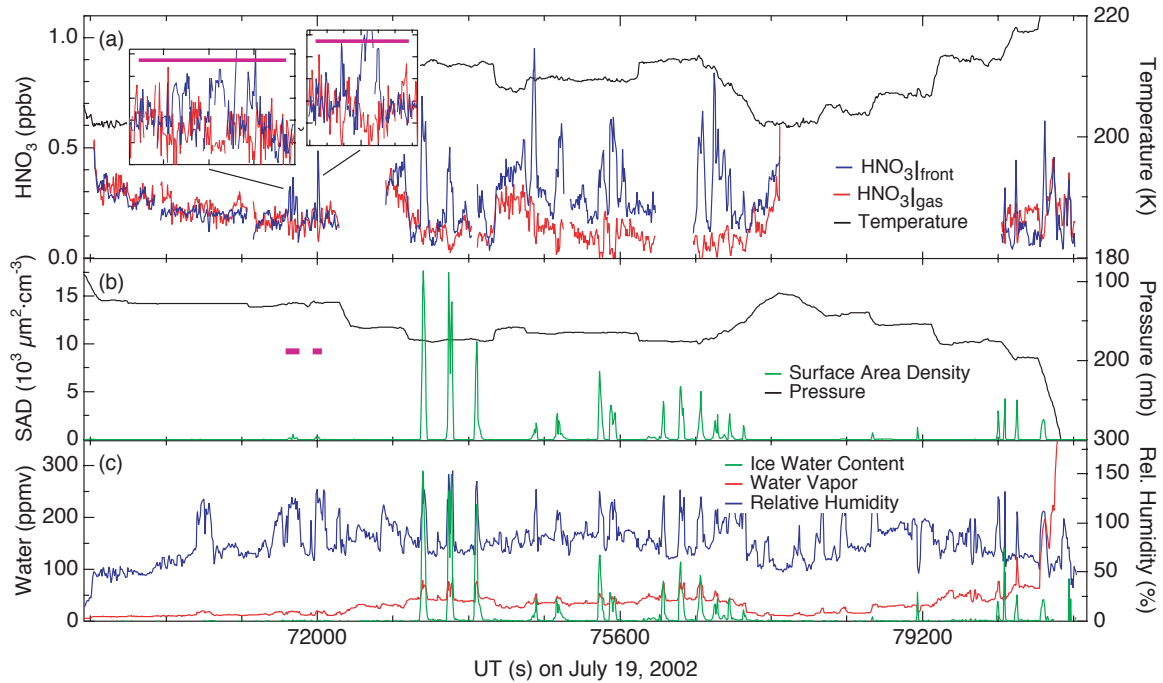


Fig. 4 Popp et al.

**Figure 4.** Same as Fig. 2, for the flight on July 19, 2002. Purple bars in panel (b) represent 2 flight segments in which cirrus clouds formed in the contrail of the WB-57F were observed. The insets in panel (a) shows 1-s averages of  $\text{HNO}_3$  front and  $\text{HNO}_3$  gas during the two contrail intercepts. The purple bars in the first and second insets represent the same time periods as the first and second purple bars in panel (b). The vertical scale on the inset panels is 0 to 0.5 ppbv.

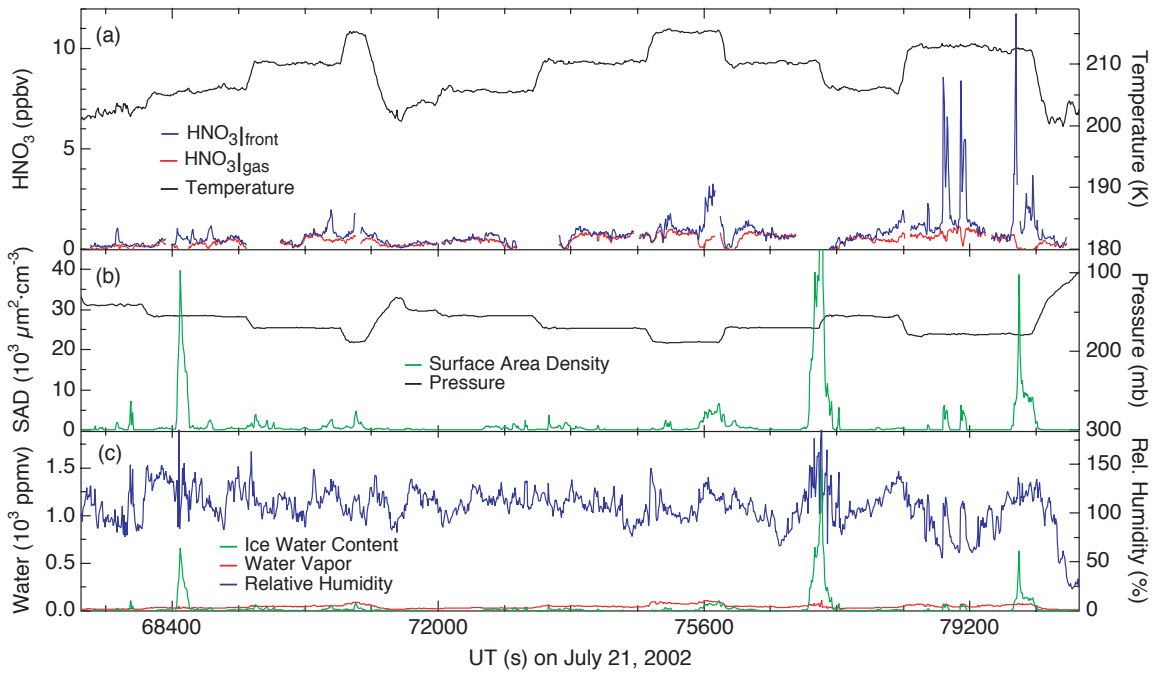


Fig. 5 Popp et al.

**Figure 5.** Same as Fig. 2, for the flight on July 21, 2002.

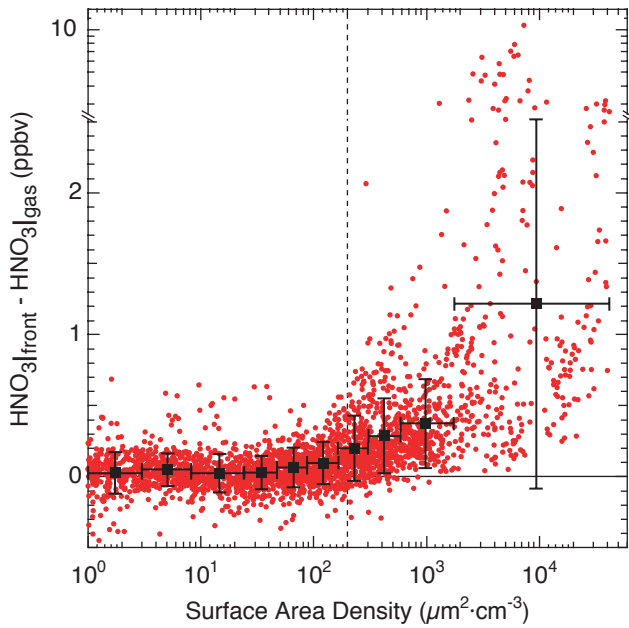


Fig. 6 Popp et al.

**Figure 6.** ( $\text{HNO}_3|_{\text{front}} - \text{HNO}_3|_{\text{gas}}$ ) vs. SAD for the flights of July 11, 13, 19 and 21, 2002. Values of ( $\text{HNO}_3|_{\text{front}} - \text{HNO}_3|_{\text{gas}}$ ) are proportional, but not equal to condensed-phase  $\text{HNO}_3$  ( $\text{HNO}_3|_{\text{con}}$ ) because they do not include a correction for particle oversampling in the front channel inlet. Red circles represent 10-s averages and black squares represent mean values of the 10-s data grouped into deciles. Vertical bars represent the standard deviation about the mean value in each decile, and horizontal bars indicate the upper and lower boundaries of each decile. Note that the vertical axis is shown with a logarithmic scale at values greater than 2.5. The dashed vertical line at the SAD of  $200 \mu\text{m}^2\cdot\text{cm}^{-3}$  represents the lower limit chosen here to represent measurements made in cirrus clouds.

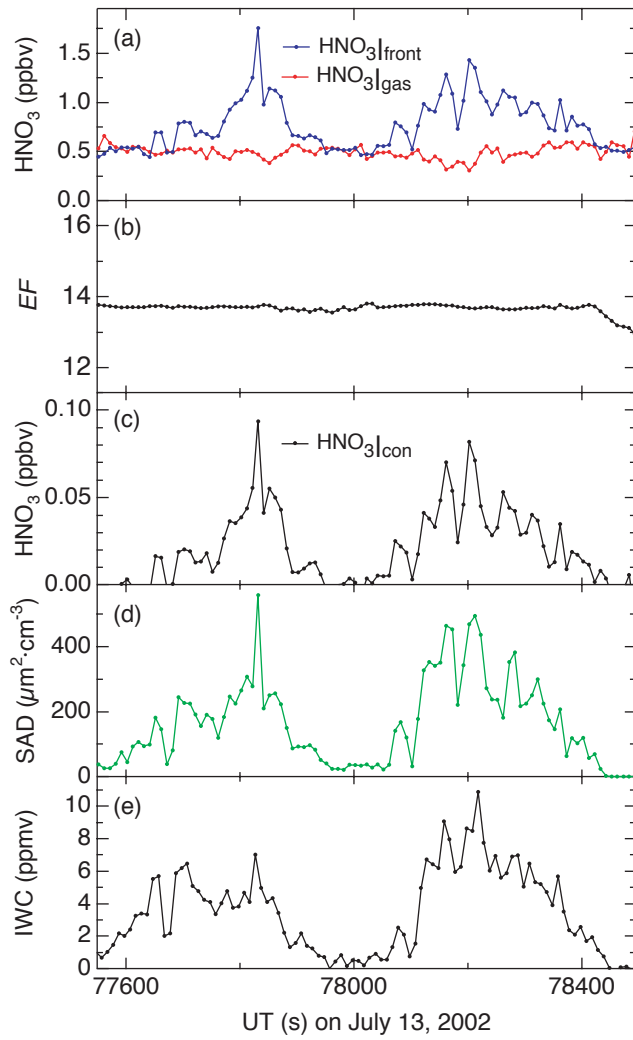


Fig. 7 Popp et al.

**Figure 7.** Calculation of  $\text{HNO}_3|_{\text{con}}$  for a cirrus cloud encounter by the NASA WB-57F on July 13, 2002, showing  $\text{HNO}_3|_{\text{front}}$  and  $\text{HNO}_3|_{\text{gas}}$  (panel a),  $EF$  (panel b),  $\text{HNO}_3|_{\text{con}}$  (panel c), SAD (panel d) and IWC (panel e). All data are shown as 10-s averages. The horizontal axis spans approximately 16 minutes and 180 km of flight.

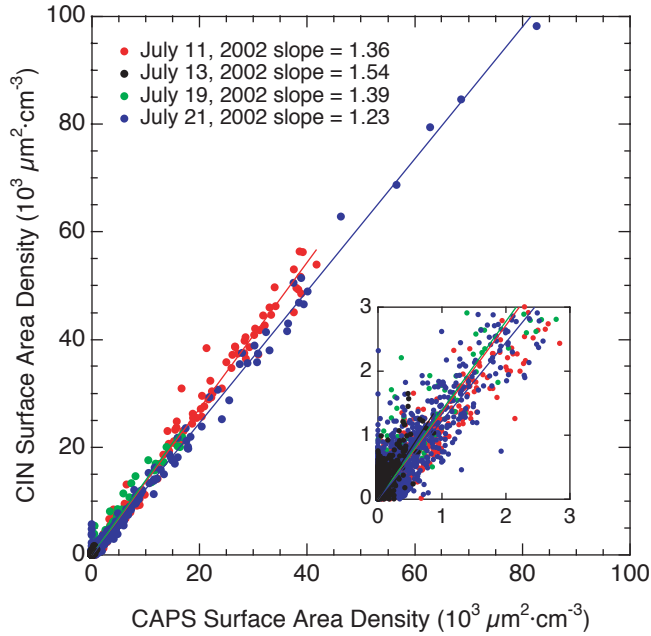


Fig. 8 Popp et al.

**Figure 8.** Comparison of CIN- and CAPS-derived SAD measured during the flights of July 11, 13, 19 and 21, 2002. Data at SADs less than  $3 \mu\text{m}^2\cdot\text{cm}^{-3}$  are expanded in the inset. All data are shown as 10-s averages. Lines represent a least-squares fit to the data for each flight date. The slope of the linear fit (constrained through the origin) is shown for each flight date in the figure legend.

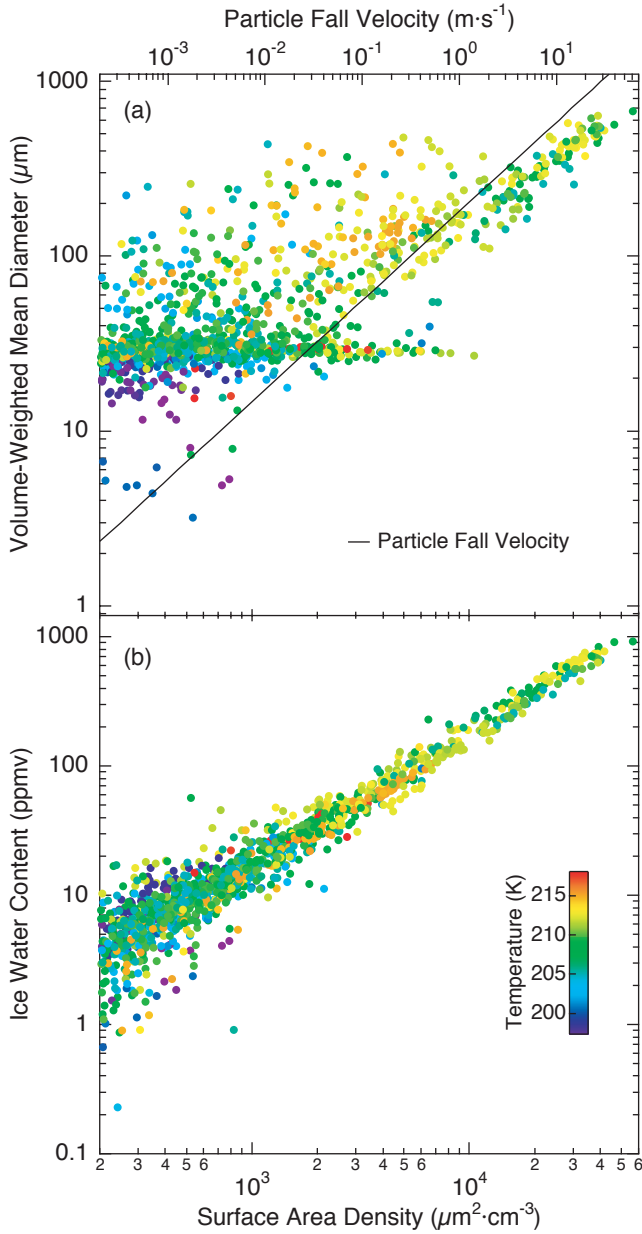


Fig. 9 Popp et al.

**Figure 9.** Panel (a). Volume-weighted mean diameter of cirrus cloud particles vs. SAD measured during the flights on July 11, 13, 19 and 21, 2002. Only data at SADs greater than  $200 \mu\text{m}^2\cdot\text{cm}^{-3}$  are shown. Data are colored according to ambient temperature. The black line represents the terminal fall velocity for ice particles in the upper troposphere, calculated according to *Meier and Hendricks* [2002]. Panel (b). IWC (represented as a gas-phase equivalent volume mixing ratio) vs. SAD. At 130 hPa and 200 K, an IWC of 100 ppmv is equivalent to an ice water concentration of  $14 \text{ mg}\cdot\text{m}^{-3}$ . Other details same as panel (a).

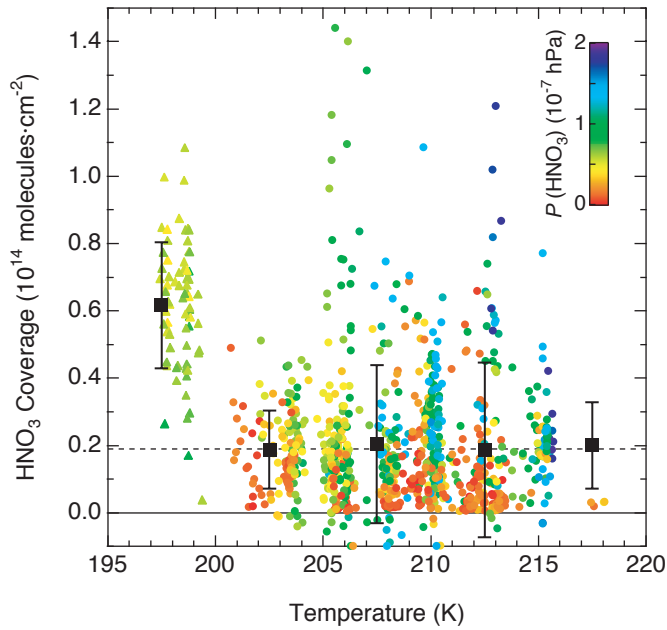


Fig. 10 Popp et al.

**Figure 10.** HNO<sub>3</sub> coverage vs. temperature for measurements made in cirrus clouds at SADs greater than 200  $\mu\text{m}^2\cdot\text{cm}^{-3}$  on July 11, 13, 19 and 21, 2002. Symbols are colored according to  $P(\text{HNO}_3)$ . Triangles at temperatures less than 200 K indicate measurements made under conditions in which NAT is stable. Mean values of HNO<sub>3</sub> coverage are plotted at the mean of 5 K temperature bins from 195 K to 220 K (black squares). Error bars represent the standard deviation in each temperature bin. Negative values of HNO<sub>3</sub> coverage are included in the calculation of the mean values. The dashed line at  $1.9\cdot 10^{13}$  molecules·cm<sup>-2</sup> represents the mean HNO<sub>3</sub> coverage observed during CRYSTAL-FACE. A complete HNO<sub>3</sub> monolayer is formed when the coverage reaches  $1.0\cdot 10^{15}$  molecules·cm<sup>-2</sup>.

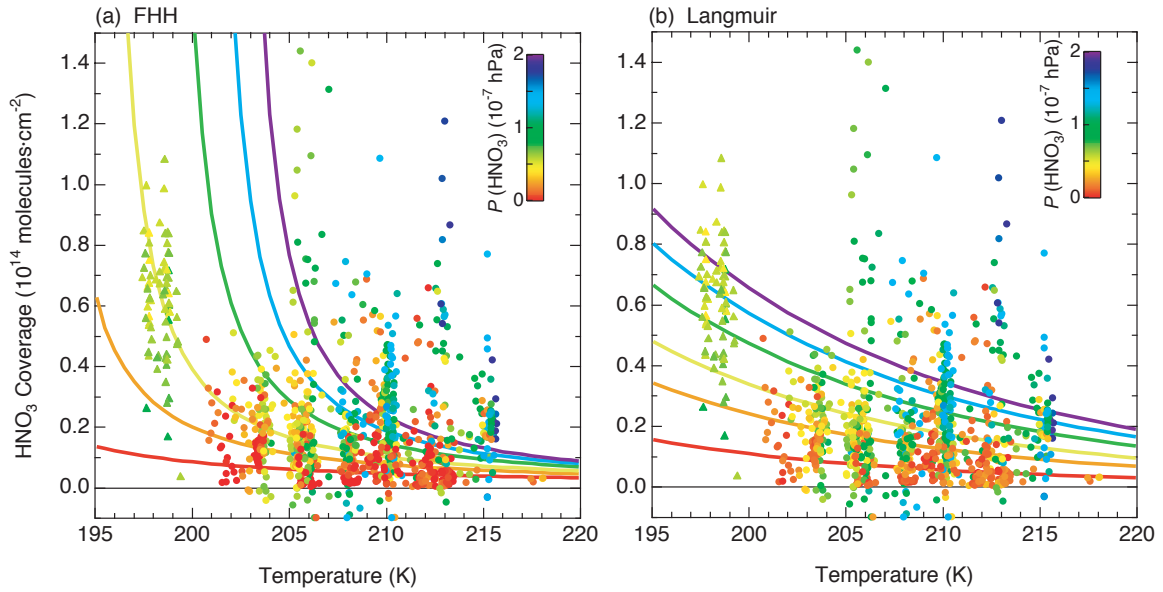


Fig. 11 Popp et al.

**Figure 11.**  $\text{HNO}_3$  coverage vs. temperature for measurements made in cirrus clouds at SADs greater than  $200 \mu\text{m}^2\cdot\text{cm}^{-3}$  on July 11, 13, 19 and 21, 2002. Symbols are colored according to  $P(\text{HNO}_3)$ . Triangles at temperatures less than 200 K indicate measurements made under conditions in which NAT is stable. Data are represented as 10-s averages. Panel (a). Lines are isobars representing  $\text{HNO}_3$  coverages calculated by the FHH  $\text{HNO}_3$  uptake model [Hudson et al., 2002] and are colored according to the same temperature scale as the observed coverages (see legend). Panel (b). Same as panel (a), except the isobars represent  $\text{HNO}_3$  coverages calculated by the Langmuir surface chemistry model.

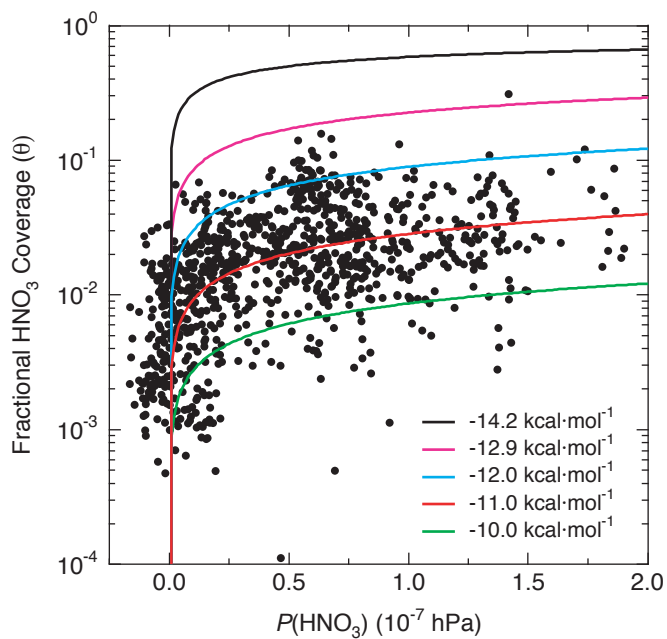


Fig. 12 Popp et al.

**Figure 12.** Fractional  $\text{HNO}_3$  surface coverage ( $\theta$ ) vs.  $P(\text{HNO}_3)$  measured during the flights of July 11, 13, 19 and 21, 2002. Colored lines are isotherms fitted according to equations (2) and (3) (see text) with values of  $\Delta H_{ads}$  shown in the legend and the median observed temperature of 208 K. All data are represented as 10-s averages for measurements made at SADs greater than  $200 \mu\text{m}^2\cdot\text{cm}^{-3}$ .

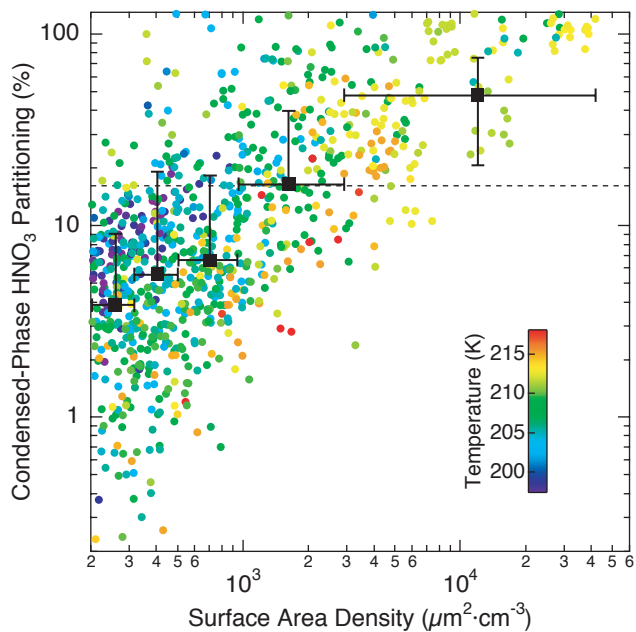


Fig. 13 Popp et al.

**Figure 13.** Fraction of total  $\text{HNO}_3$  in the condensed phase vs. SAD measured during the flights of July 11, 13, 19 and 21, 2002. Data are represented as 10-s averages for measurements made at SADs greater than  $200 \mu\text{m}^2\cdot\text{cm}^{-3}$  and are colored according to temperature. Black squares represent mean values of the 10-s data grouped into quintiles. Vertical bars represent the standard deviation about the mean value in each quintile and horizontal bars represent the upper and lower boundaries of each quintile. Values of condensed-phase partitioning greater than 100% occur when zero or near-zero  $\text{HNO}_3|_{\text{gas}}$  abundances are measured as negative values. The dashed line at 16% represents the mean value of  $\text{HNO}_3$  partitioned in the condensed phase during CRYSTAL-FACE.

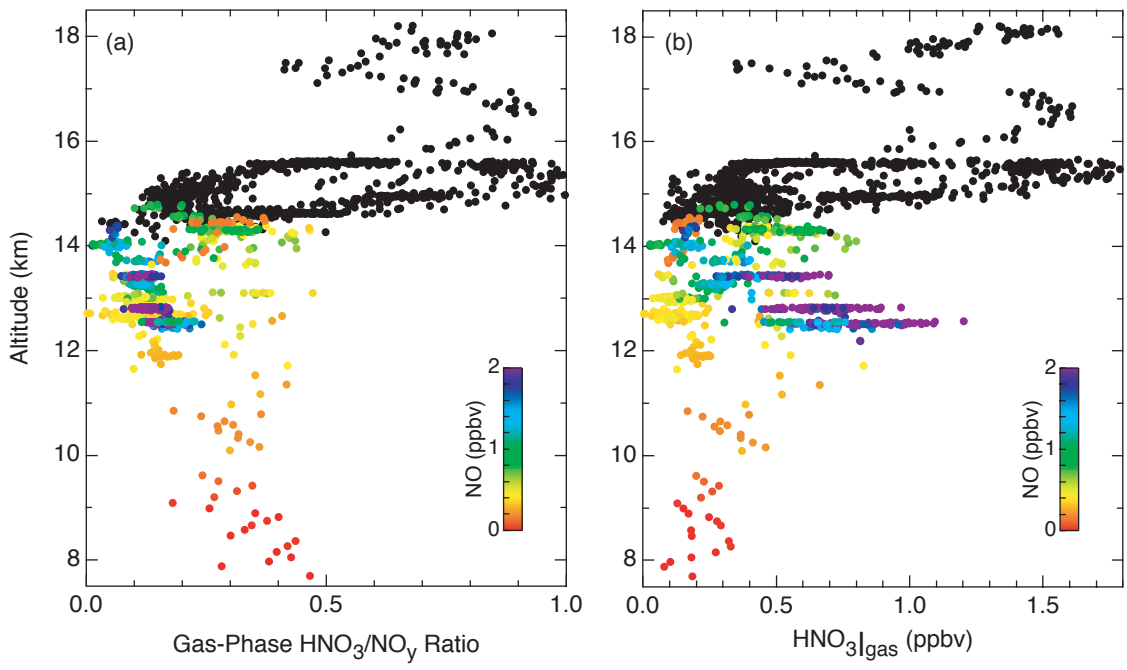


Fig. 14 Popp et al.

**Figure 14.** Panel (a). Vertical profile of the gas-phase  $\text{HNO}_3/\text{NO}_y$  ratio observed in cloud free air ( $\text{SADs} < 20 \mu\text{m}^2\cdot\text{cm}^{-3}$ ) during the flights of July 11, 13, 19 and 21, 2002. Tropospheric measurements (according to the Microwave Temperature Profiler) are colored according to measured NO. Stratospheric measurements are shown in black. Panel (b). Vertical profile of  $\text{HNO}_3|_{\text{gas}}$ . Other details same as panel (a).